Electronic Supplementary Material (ESI) for Journal of Materials Chemistry A.

Supporting information

Simultaneous Upcycling of PET Plastic Waste and CO_2 Reduction through Co-electrolysis: A Novel Approach Integrating CO_2 Reduction and PET Hydrolysate Oxidation

Kilaparthi Sravan Kumar[1], Ahmed Addad[2], Alexandre Barras[1], Sabine Szunerits[1], and Rabah Boukherroub[1]*

[1]*Univ. Lille, CNRS, Univ. Polytechnique Hauts-de-France, UMR 8520 - IEMN, F-59000 Lille, France*

[2]*Univ. Lille, CNRS, UMR 8207 - UMET, F-59000 Lille, France*

Corresponding author: rabah.boukherroub@univ-lille.fr

Characterization

Scanning electron microscopy (SEM) images, energy-dispersive X-ray spectroscopy analysis (EDX) data and EDX mapping images were obtained using a JEOL JSM-7800F field-emission scanning electron microscope (SEM) operated at 15 kV. X-ray diffraction (XRD) patterns were collected on a high flux Rigaku Smartlab rotated anode, working with a copper Kα radiation (1.5418 Å) at an applied voltage of 45 kV and an anode current of 200 mA in the 2θ range of 5–90°. Raman measurements were performed on a LabRam HR Micro-Raman system (Horiba Jobin Yvon) using a 473 nm laser diode as excitation source. The chemical composition of all materials was analyzed by X-ray photoelectron spectroscopy (XPS) using an ESCALAB 220 XL spectrometer from Vacuum generators featuring a monochromatic Al Kα X-ray source at 1486.6 eV. Ultraviolet-visible (UV-vis) spectra were recorded by using Safas Bio-UVmc² spectrophotometer using a quartz cell (1 cm path length) and tungsten-halogen source. Absorption spectra were recorded from 200 to 800 nm at room temperature. Fourier-transform infrared spectroscopy (FTIR) analysis was performed on a Thermo Fisher Scientific (Nicolet 8700) instrument equipped with IR solution software. FTIR spectra were recorded at 6 cm^{-1} spectral resolution in the frequency range of 700–4000 cm^{-1} at room temperature.

The ^{1}H and ^{13}C NMR spectra were collected on a Bruker 300 MHz. The samples for NMR analysis were prepared by mixing 550 µL of electrolyte with 50 µL of D_2O. Water suppression method was used in all ^{1}H NMR experiments.

Mechanism of formation of $Bi_2O_2CO_3$ (BOC) nanosheets

When $BiPO_4$@rGO electrode was immersed in a 0.5M $KHCO_3$ solution, no morphological changes were observed. However, when a potential of -0.8 V *vs.* RHE was applied for 1 h, *in situ*

transformation was seen. The following series of chemical reactions (1-5) could be responsible for the formation of BOC nanosheets.

$$CO_2 + H_2O + 2e^- \rightarrow HCOO^- + OH^- \quad (1)$$

$$CO_2 + H_2O + 2e^- \rightarrow CO + 2OH^- \quad (2)$$

$$2H_2O + 2e^- \rightarrow H_2 + 2OH^- \quad (3)$$

$$Bi^{3+} + 3OH^- \rightarrow Bi(OH)_3 \quad (4)$$

$$2Bi(OH)_3 + CO_2 \rightarrow Bi_2O_2CO_3 + 3H_2O \quad (5)$$

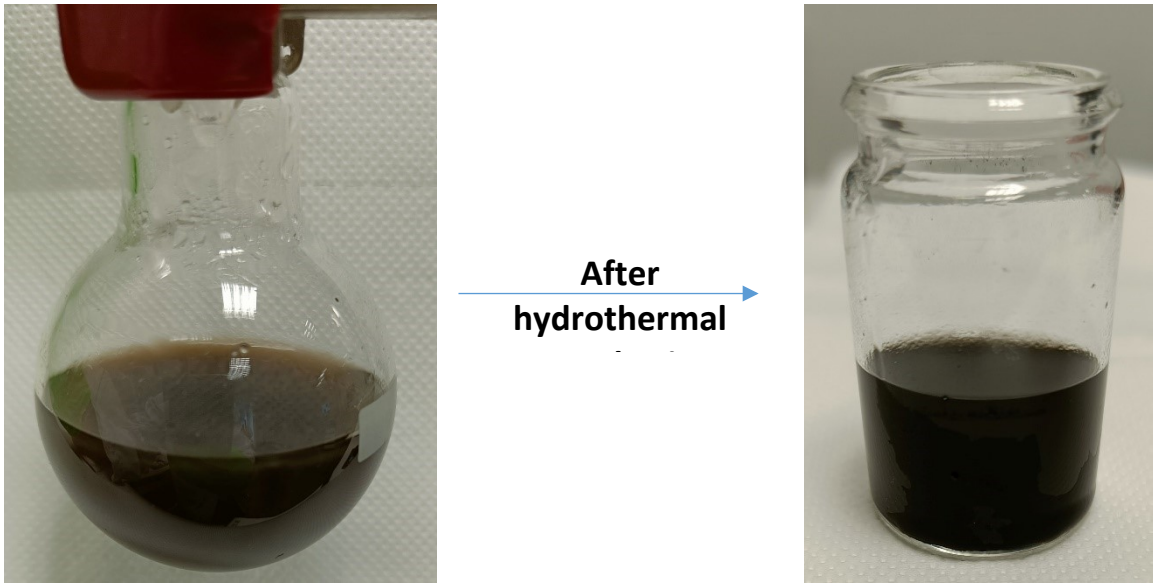

Figure S1. Color change from dark brown to black before (left) and after (right) hydrothermal reaction at 160 °C for 16h.

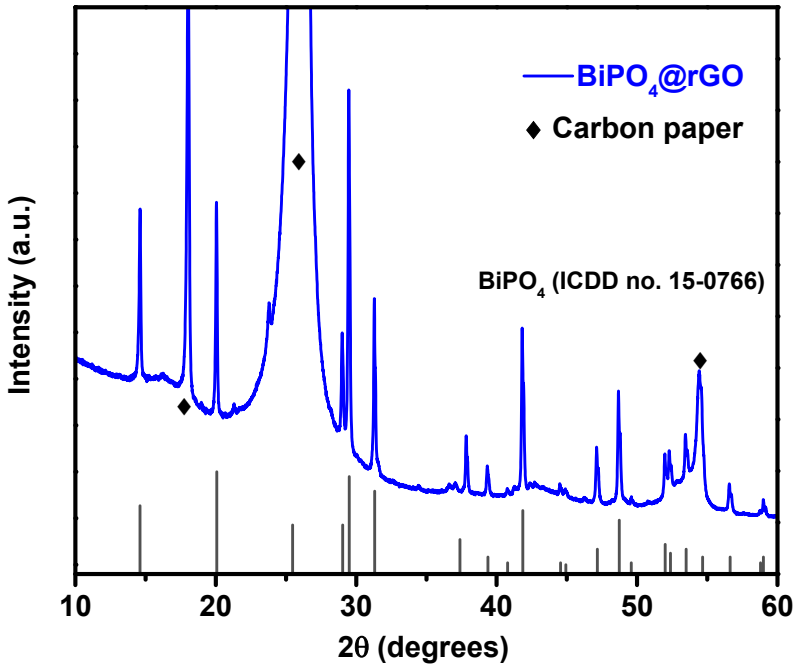

Figure S2. X-ray diffraction (XRD) pattern of the as-prepared $BiPO_4$@rGO product.

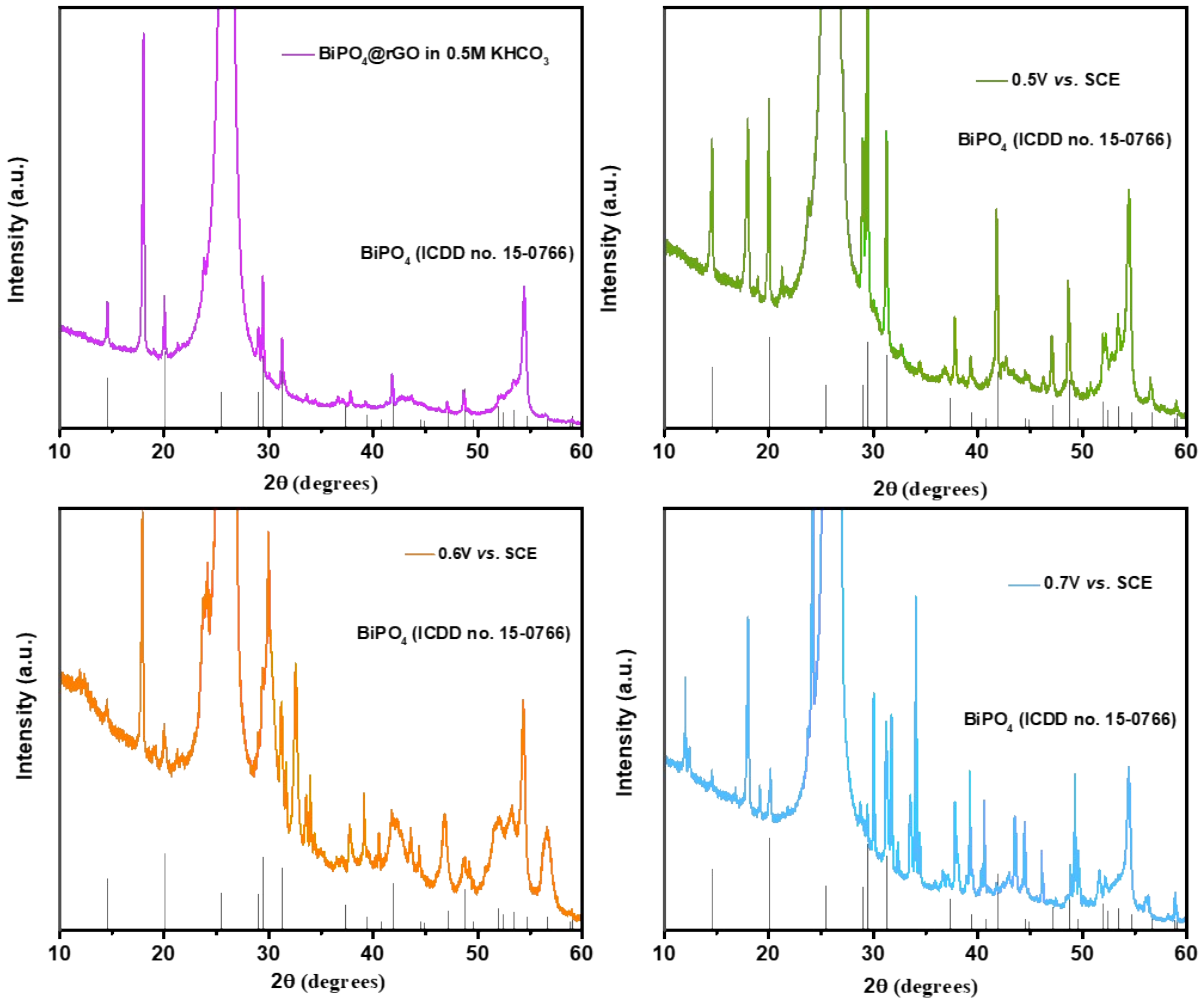

Figure S3. XRD patterns of electrochemical activation of $BiPO_4$@rGO at different applied potentials.

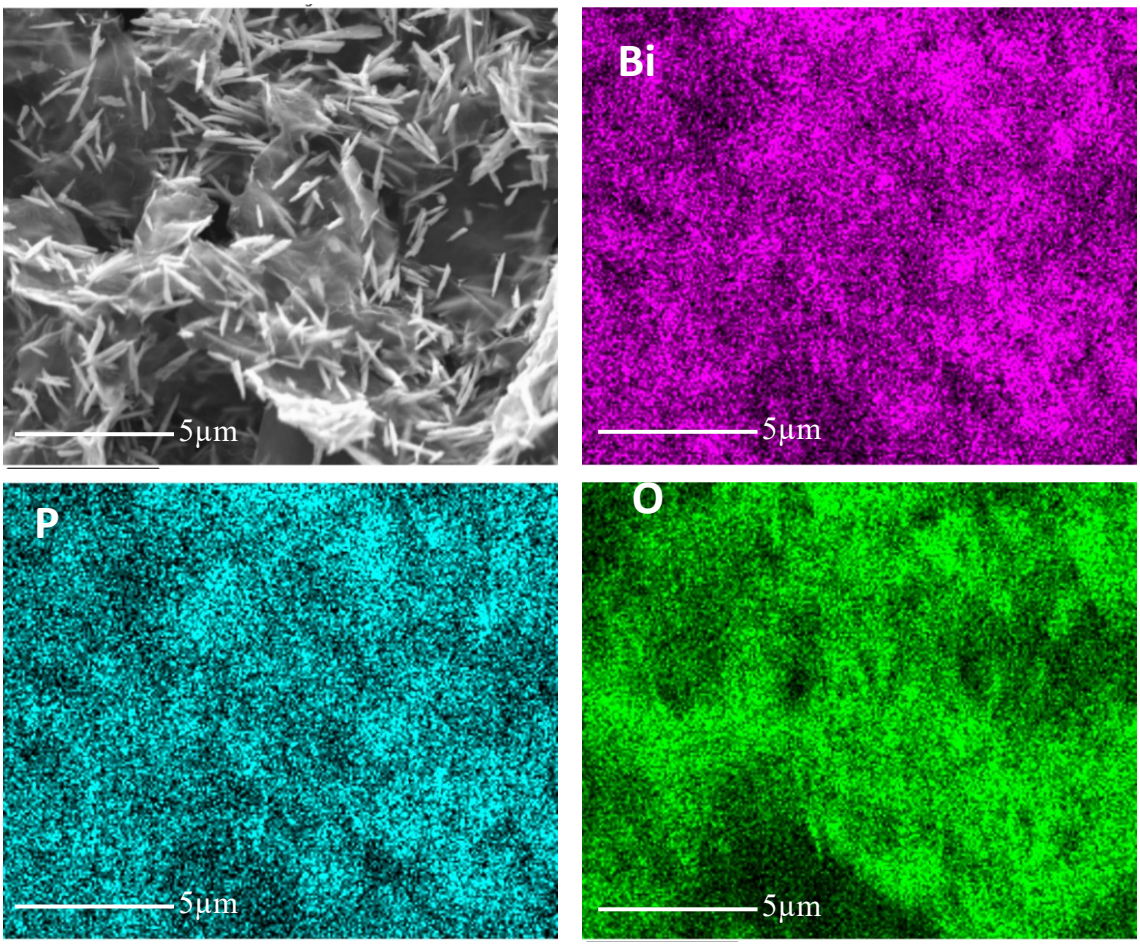

Figure S4. FESEM image and corresponding EDX mapping of Bi, P and O of $BiPO_4$@rGO.

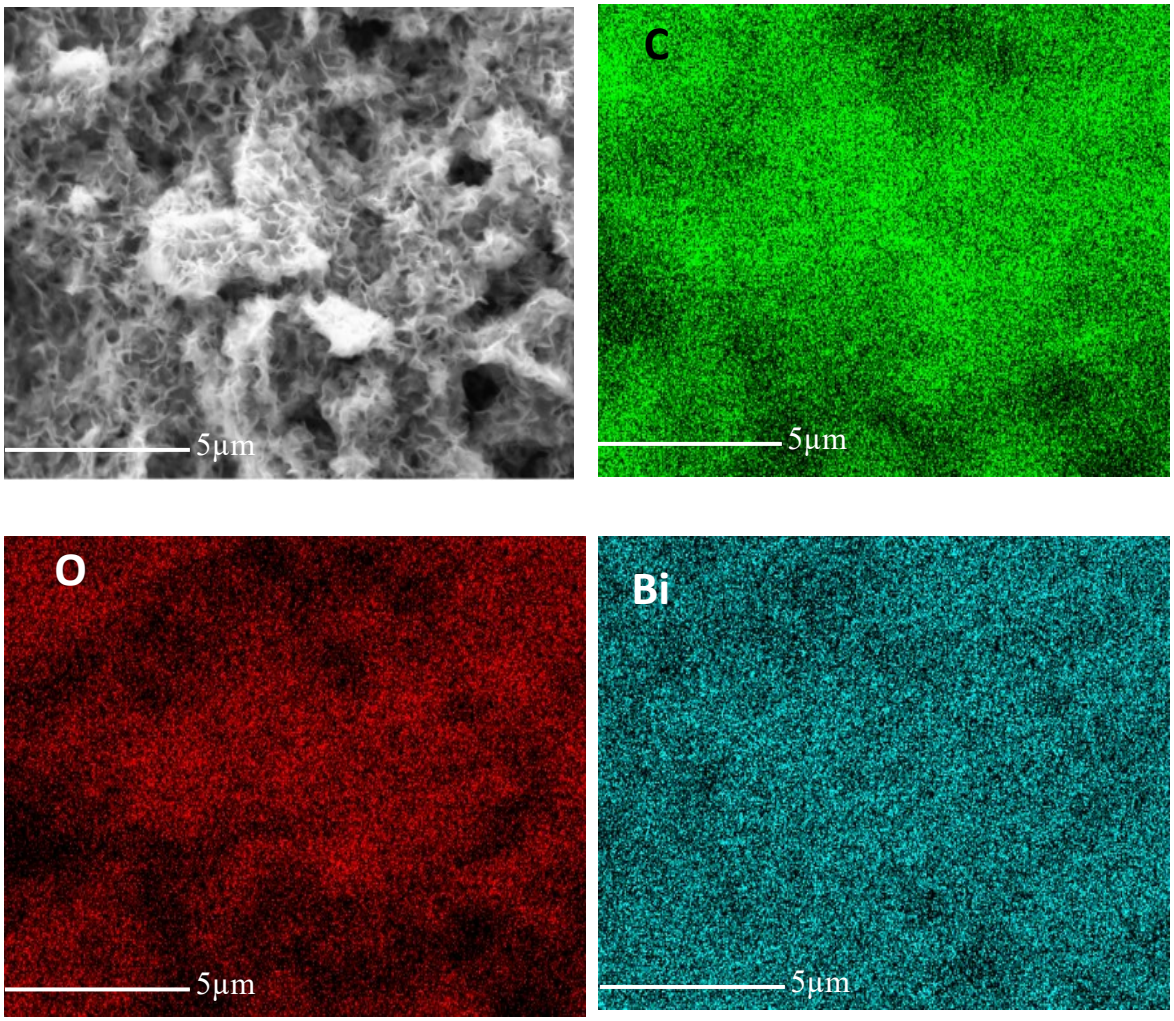

Figure S5. FESEM image and corresponding EDX mapping of C, O and Bi of BOC@rGO electrode.

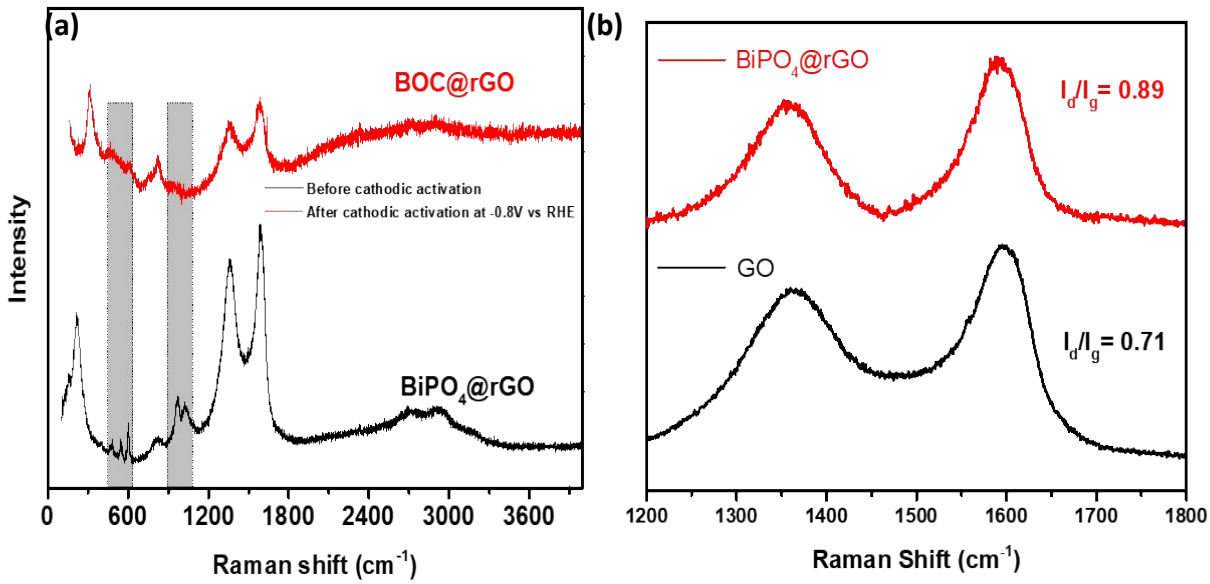

Figure S6. (**a**) Raman spectra of BOC@rGO and $BiPO_4$@rGO. (**b**) I_d/I_g band ratio determined from the Raman spectra of $BiPO_4$@rGO and GO.

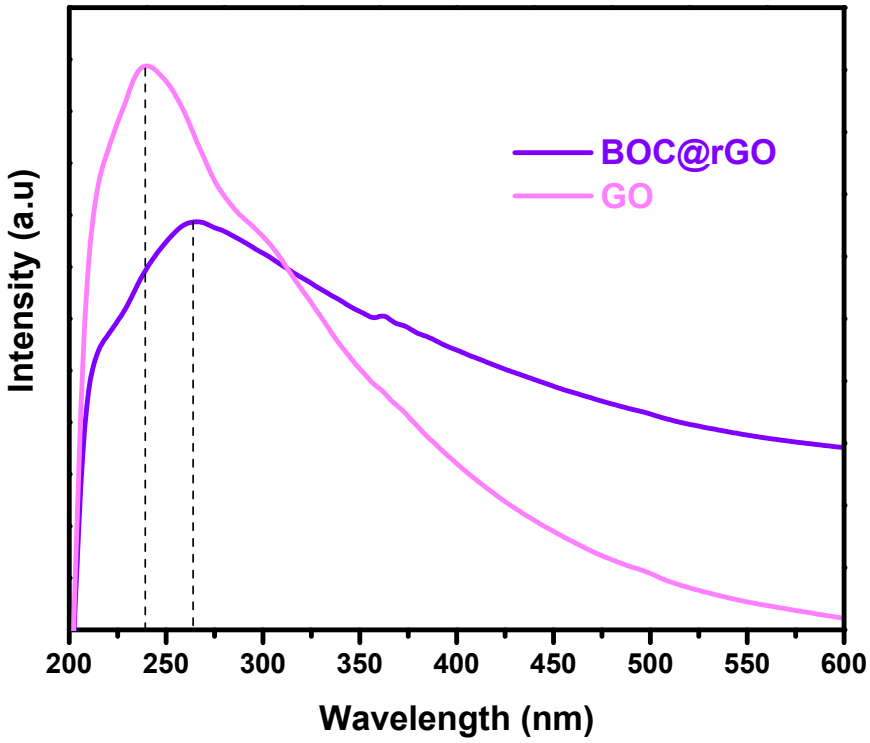

Figure S7. UV-visible absorption spectra of BOC@rGO and GO.

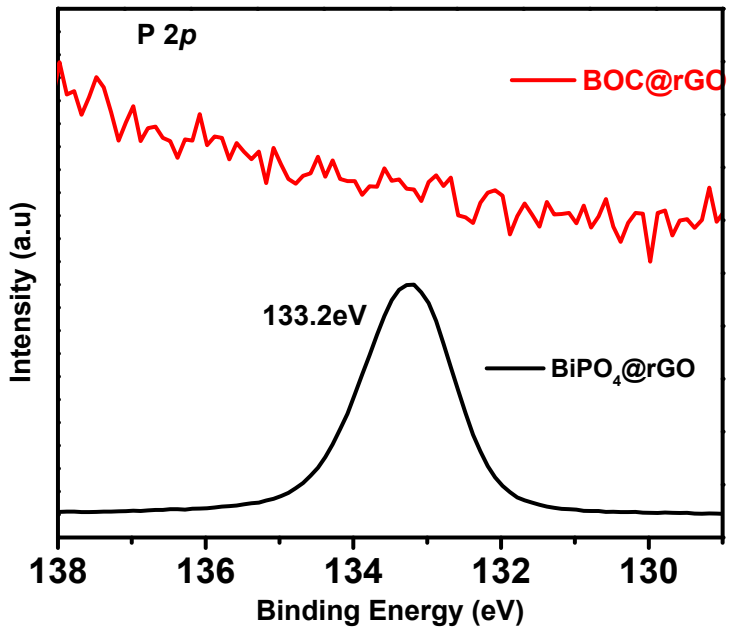

Figure S8. High resolution XPS spectra of the P 2p of BOC@rGO (black) and $BiPO_4$@rGO (red).

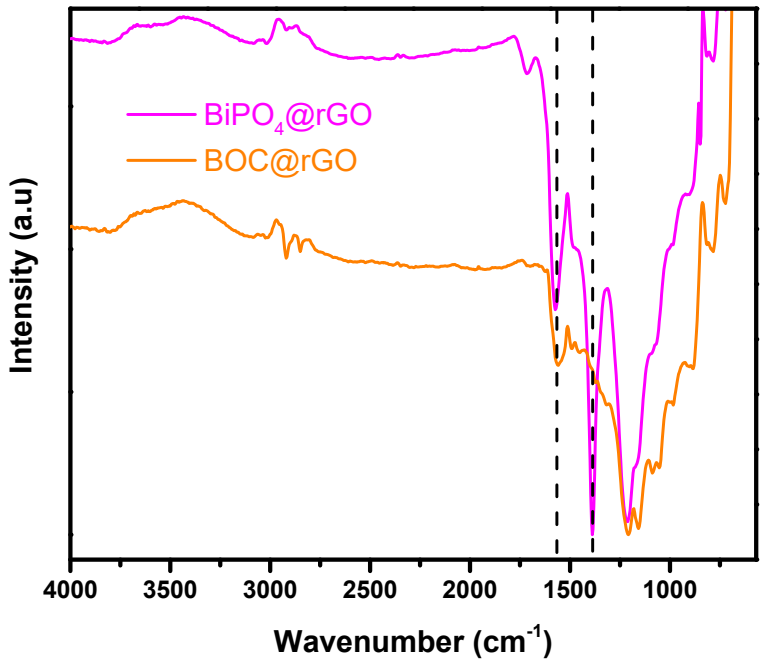

Figure S9. FTIR spectra of BOC@rGO and $BiPO_4$@rGO.

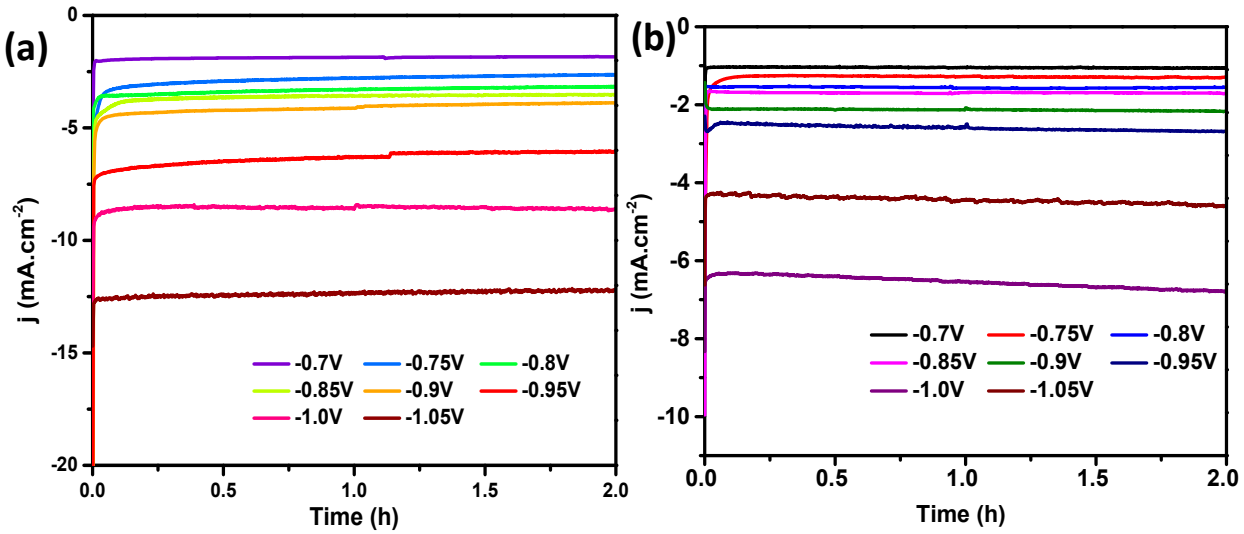

Figure S10. Chronoamperometry analysis at different potentials in CO_2-saturated 0.1 M $KHCO_3$ solution of (**a**) BOC@rGO and (**b**) BOC.

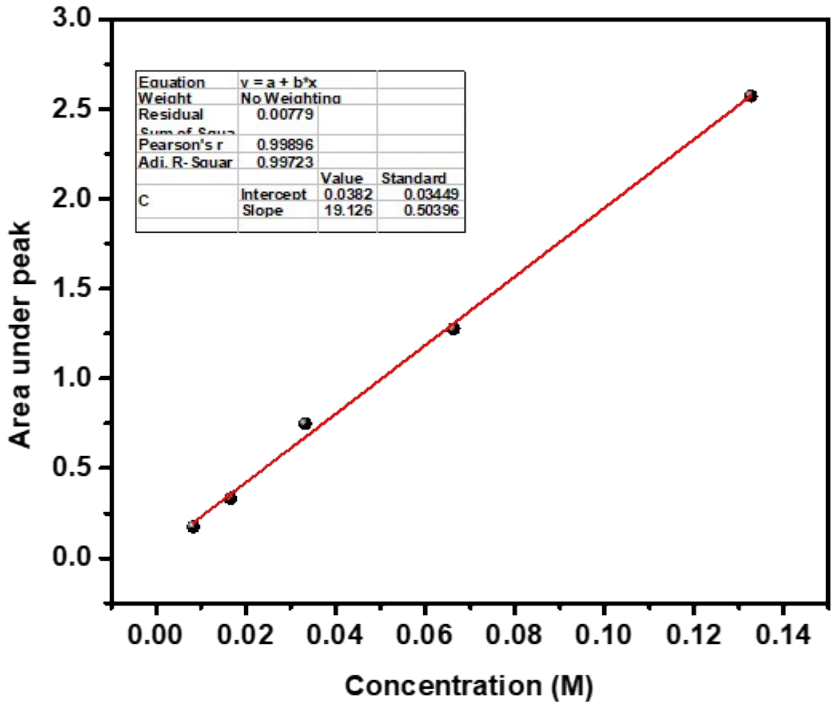

Figure S11. Calibration curve for formate concentration determined by ^1H NMR for CO_2RR.

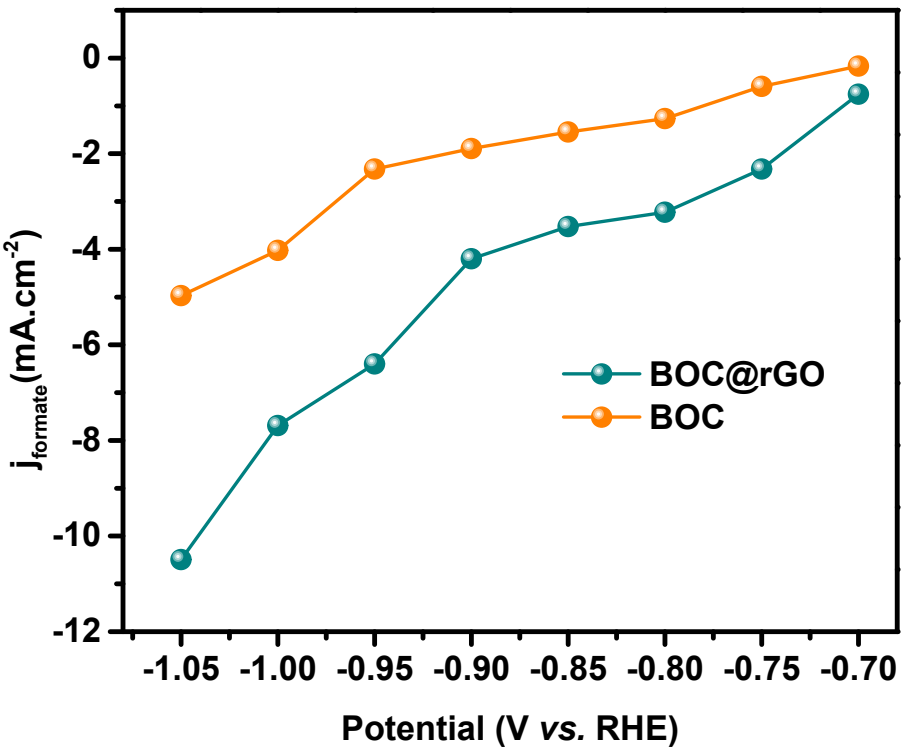

Figure S12. Partial current densities for HCOOH production of BOC@rGO and BOC.

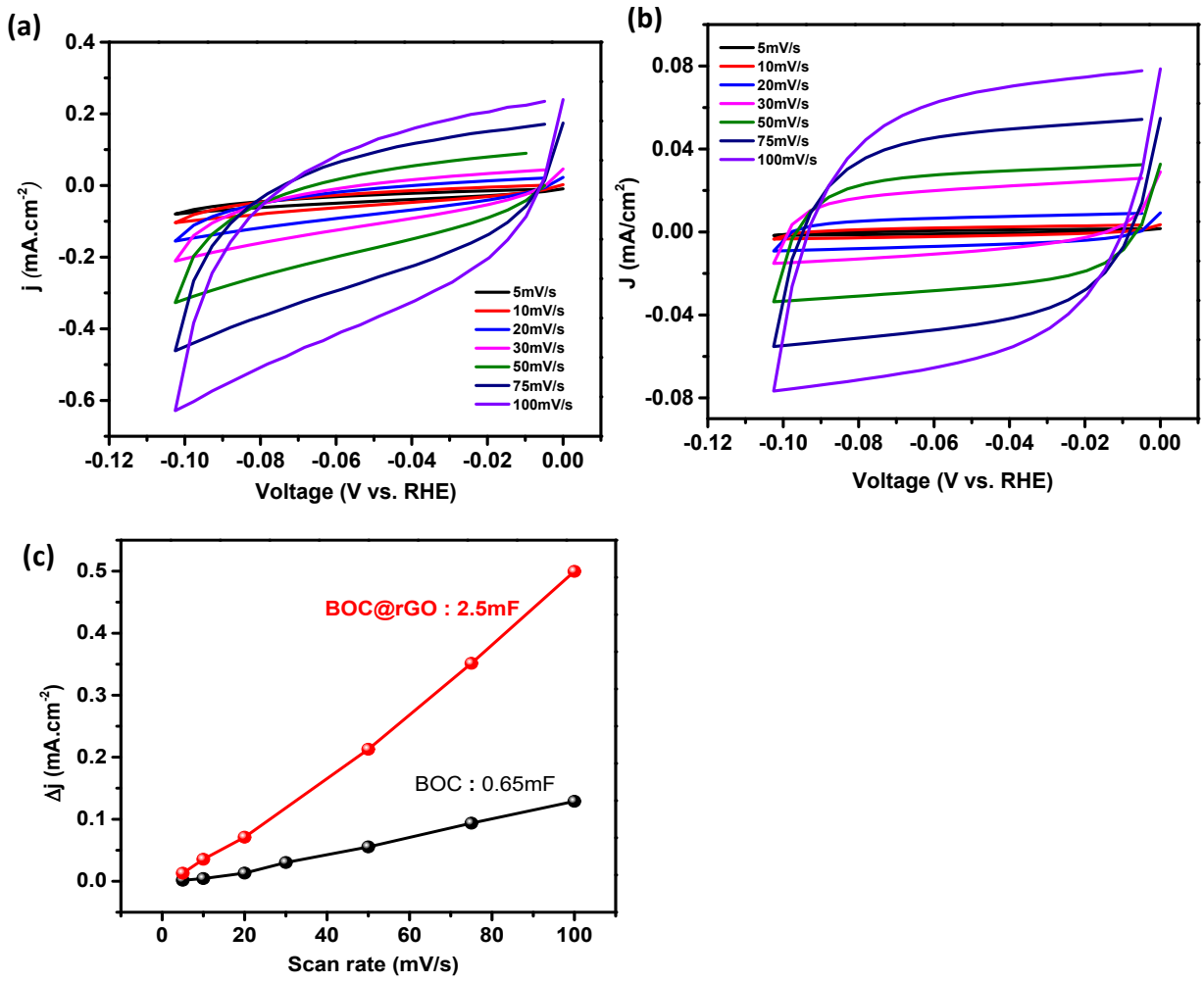

Figure S13. (**a**) CV curves of BOC@rGO and (**b**) BOC performed at different scan rates in Ar-saturated 0.1 M $KHCO_3$ aqueous solution in non-faradaic region; (**c**) C_{dl} curves of BOC@rGO and BOC.

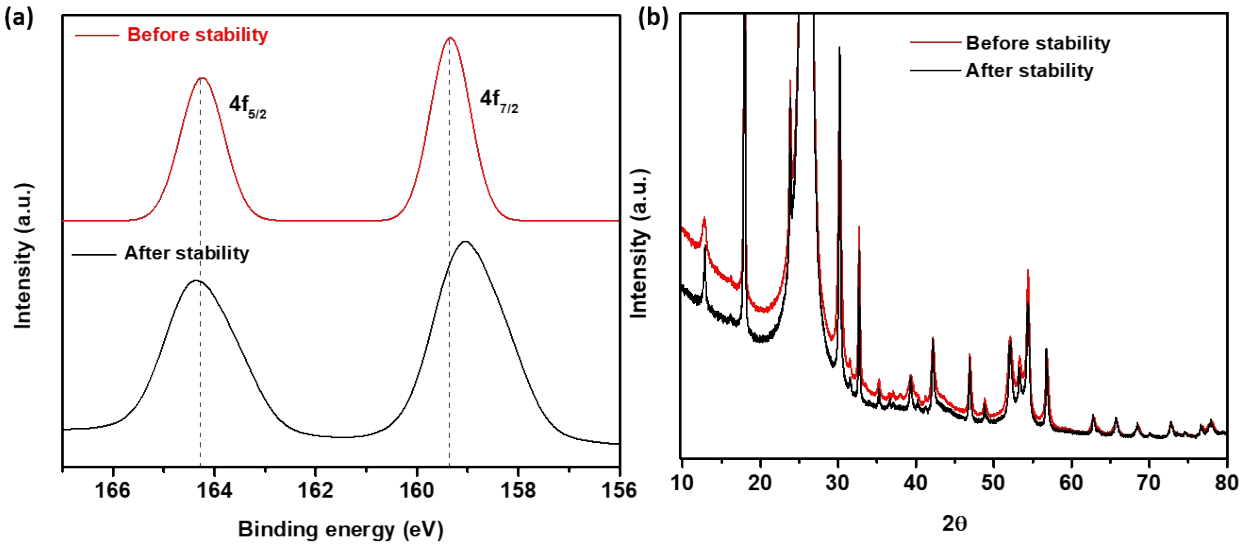

Figure S14. Bi 4f XPS spectra and XRD patterns of BOC@rGO after stability test. The spectra of as-prepared samples are shown for comparison.

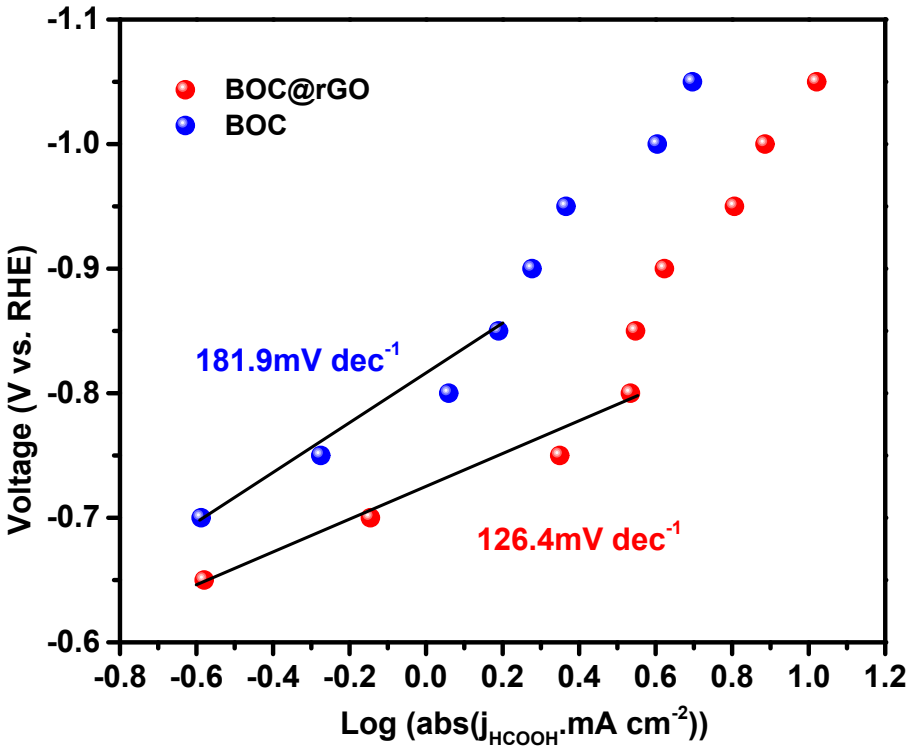

Figure S15. Tafel plots of BOC@rGO and BOC.

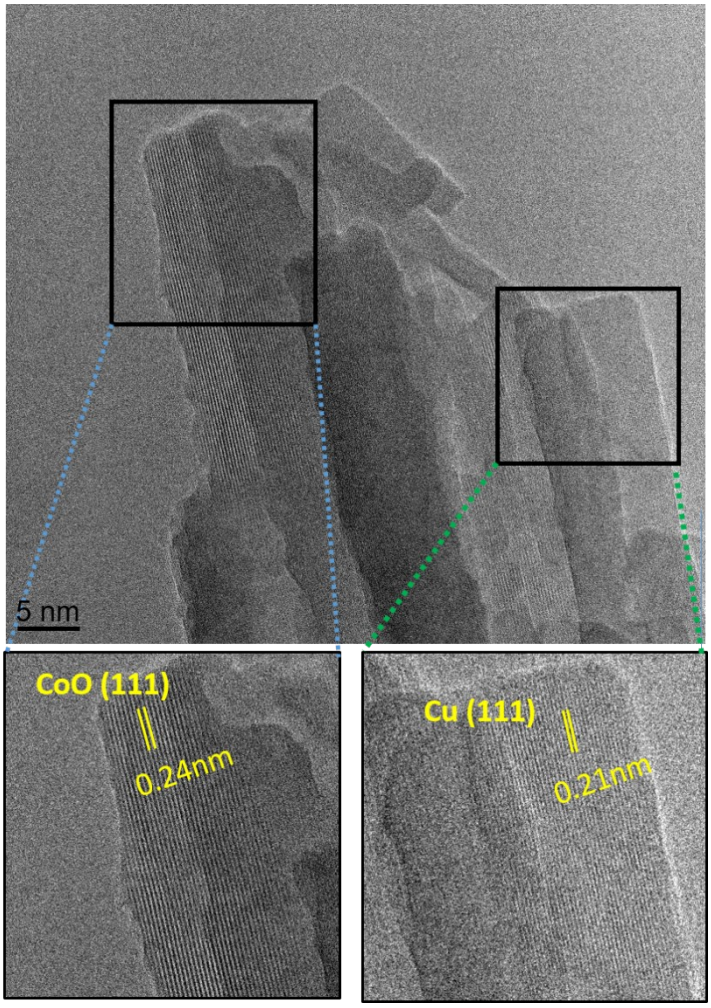

Figure S16. HR-TEM images of CuCoO@rGO nanocomposite.

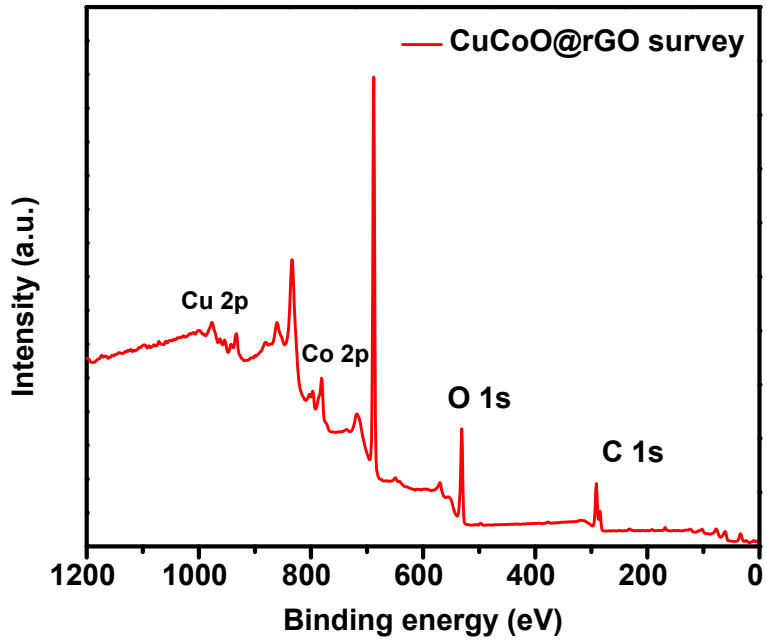

Figure S17. XPS survey spectrum of CuCoO@rGO nanocomposite.

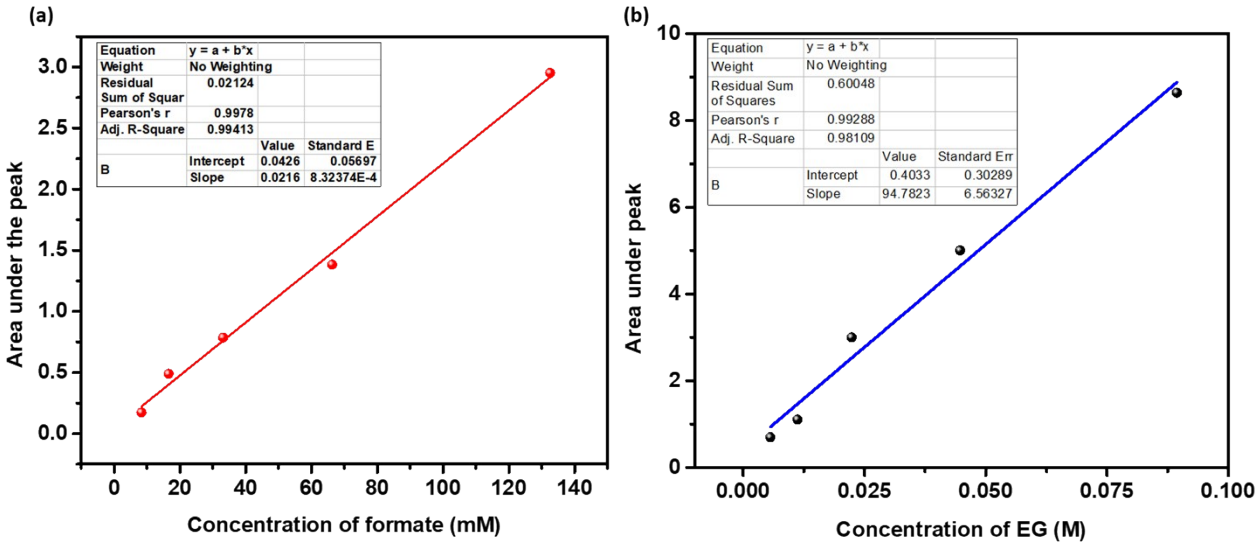

Figure S18. Calibration curves for (**a**) formate and (**b**) ethylene glycol (EG) concentrations determined by ^{1}H NMR for PET hydrolysate.

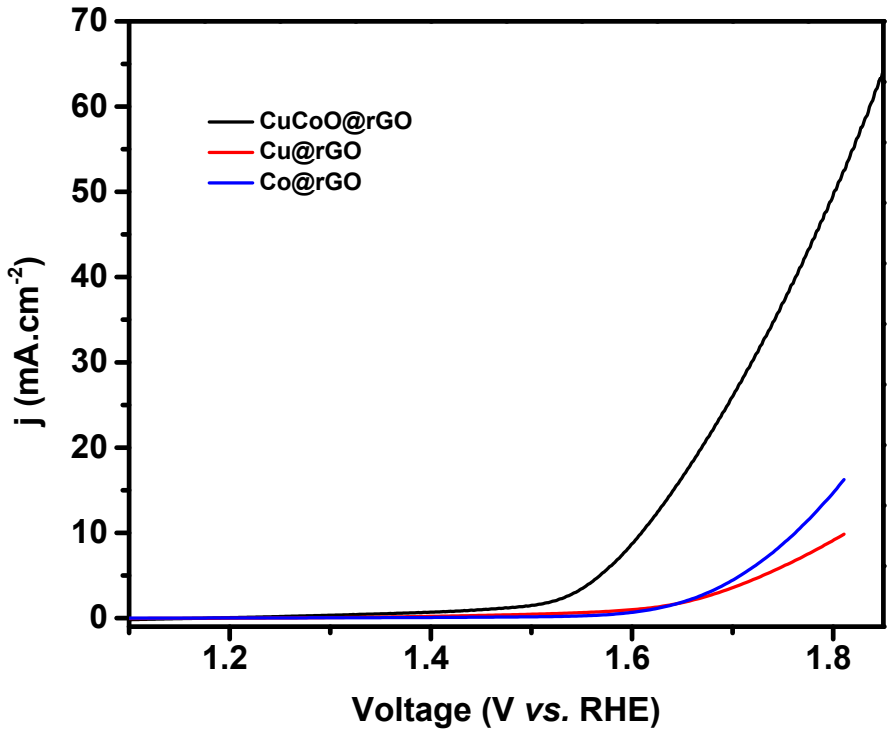

Figure S19. LSV curves of CuCoO@rGO, Cu@rGO and Co@rGO in 1 M KOH solution; scan rate =10 mV s^{-1}.

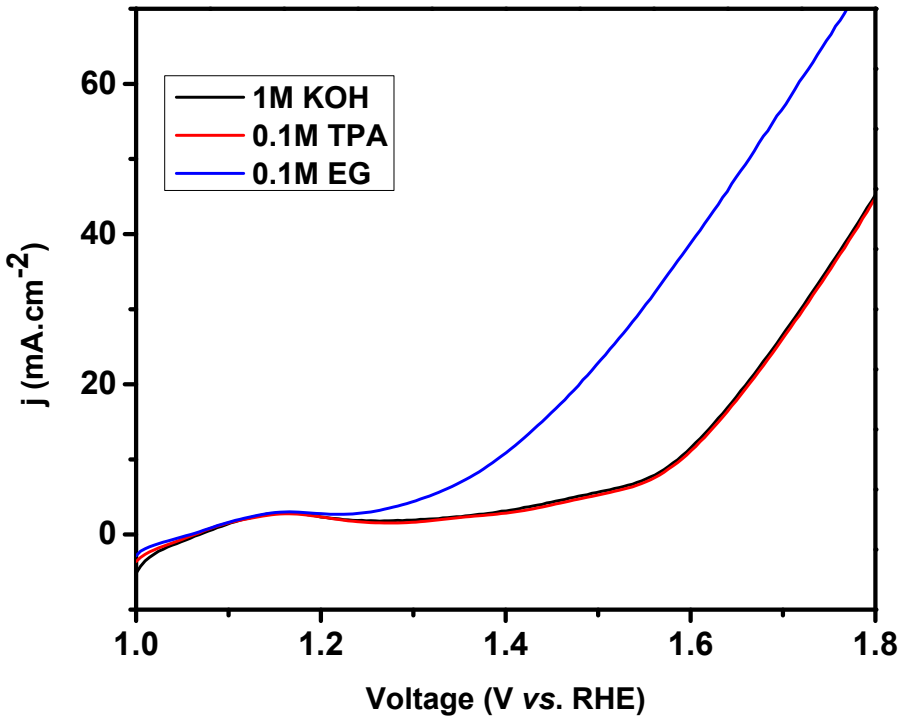

Figure S20. LSV curves of CuCoO@rGO in 1 M KOH, 0.1 M TPA and 0.1 M EG; scan rate =10 mV s^{-1}.

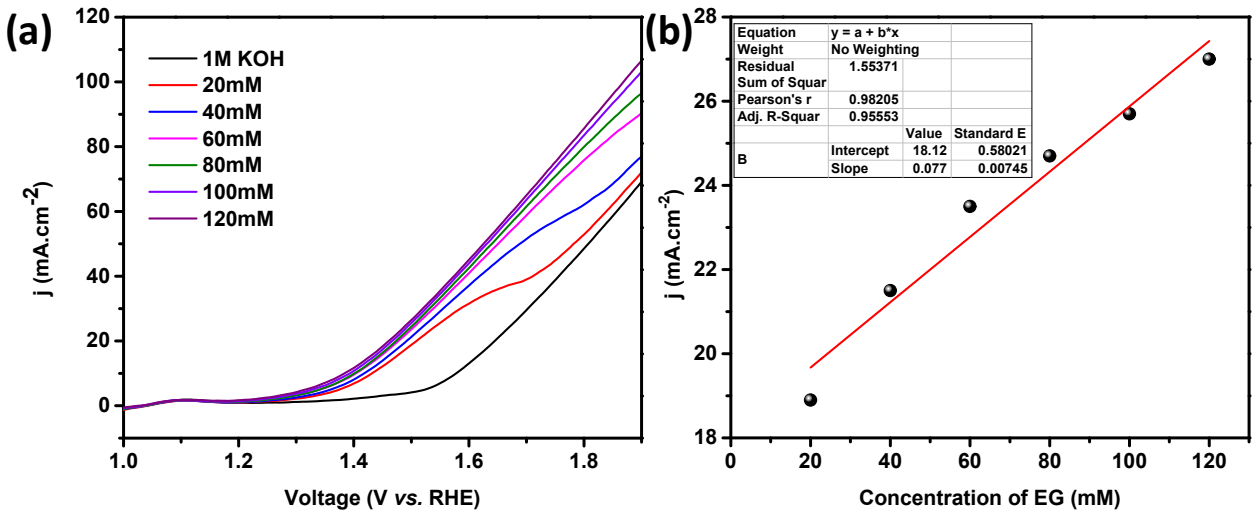

Figure S21. (**a**) LSV curves of CuCoO@rGO at varying concentrations of EG, scan rate =10 mV s^{-1}. (**b**) Linear curve of catalytic current for EG oxidation *vs.* EG concentration at 1.5 V *vs.* RHE.

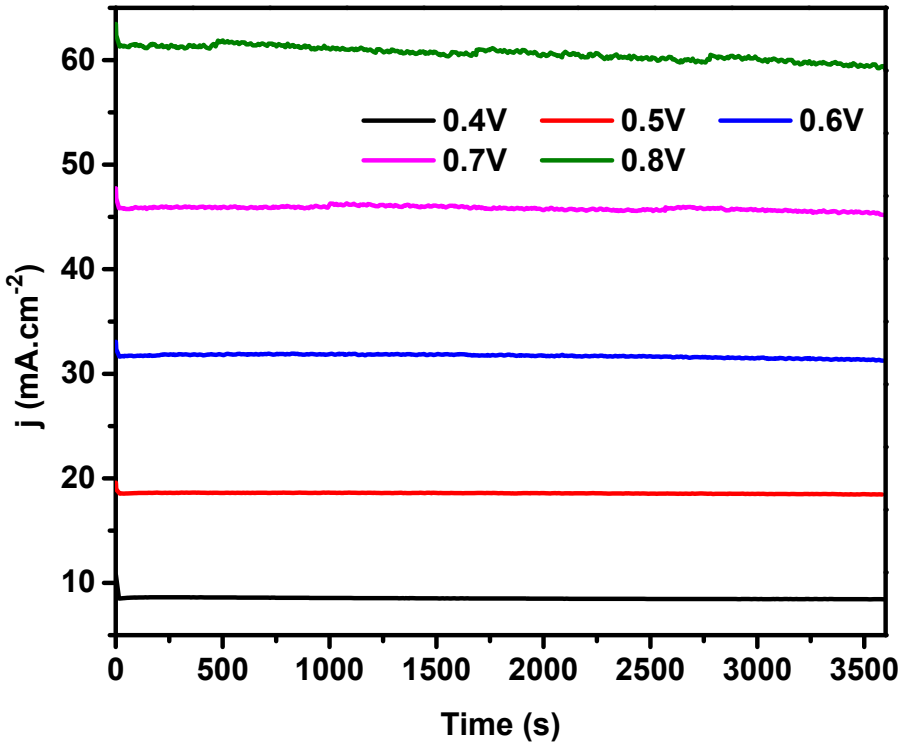

Figure S22. Controlled potential electrolysis of PET hydrolysate solution using CuCoO@rGO.

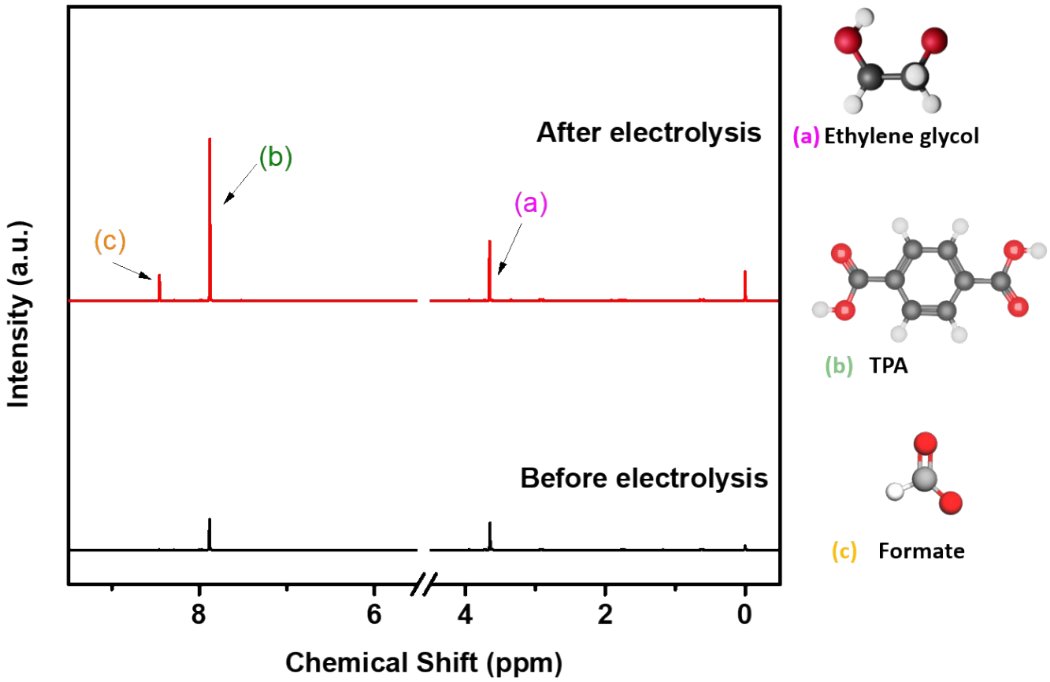

Figure S23. [1]H NMR before and after electrolysis of PET hydrolysate solution using CuCoO@rGO nanocomposite.

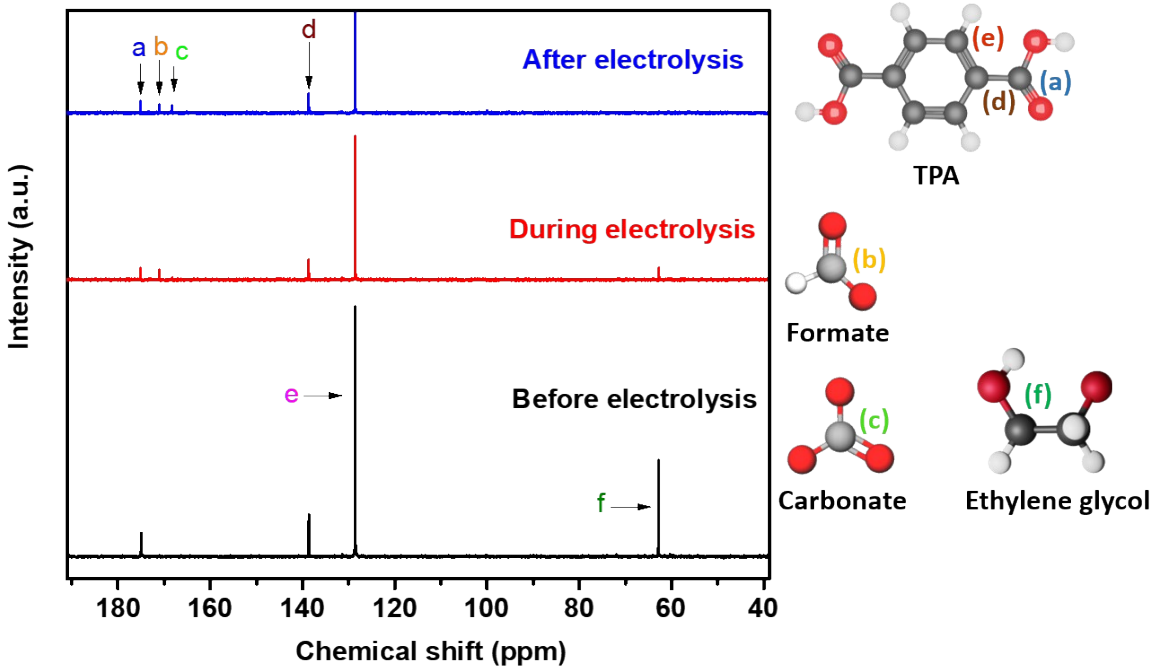

Figure S24. [13]C NMR before, during and after electrolysis of PET hydrolysate solution using CuCoO@rGO.

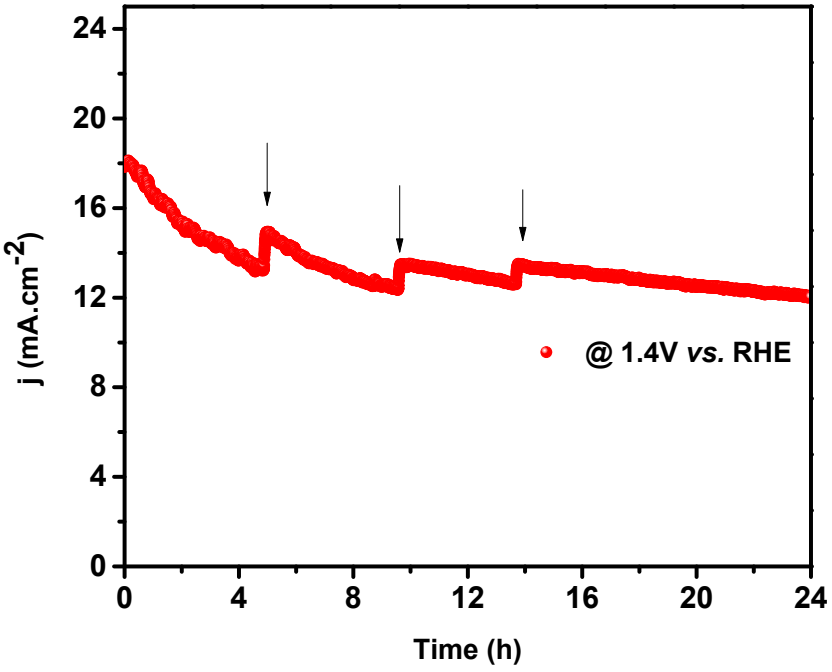

Figure S25. Long-term electrolysis upon subsequent addition of 20 mM ethylene glycol (EG) at different intervals of time.

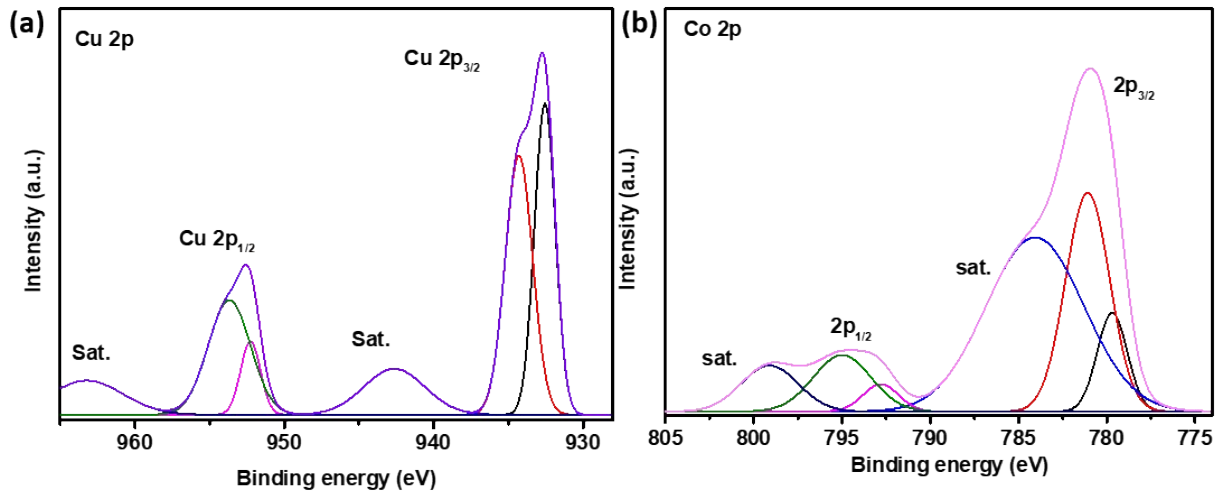

Figure S26. (**a**) Cu 2p and (**b**) Co 2p XPS spectra after electrolysis of PET hydrolysate solution using CuCoO@rGO nanocomposite.

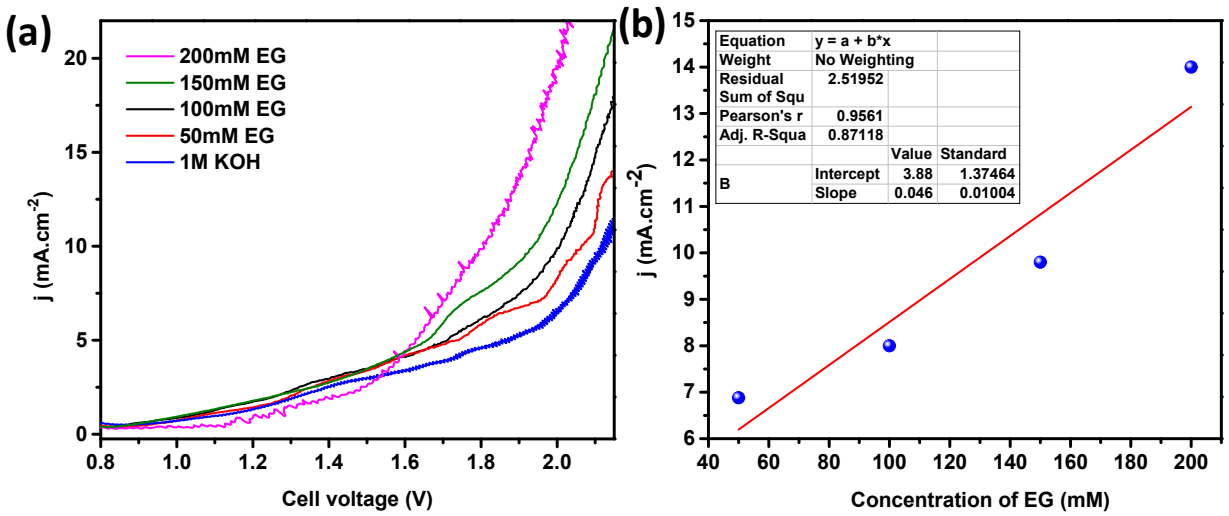

Figure S27. (**a**) LSV curves of CuCoO@rGO(+) || BOC@rGO(-) at varying concentrations of EG. (**b**) Linear curve of catalytic current for formate synthesis *vs.* EG concentration at 1.9 V cell voltage.

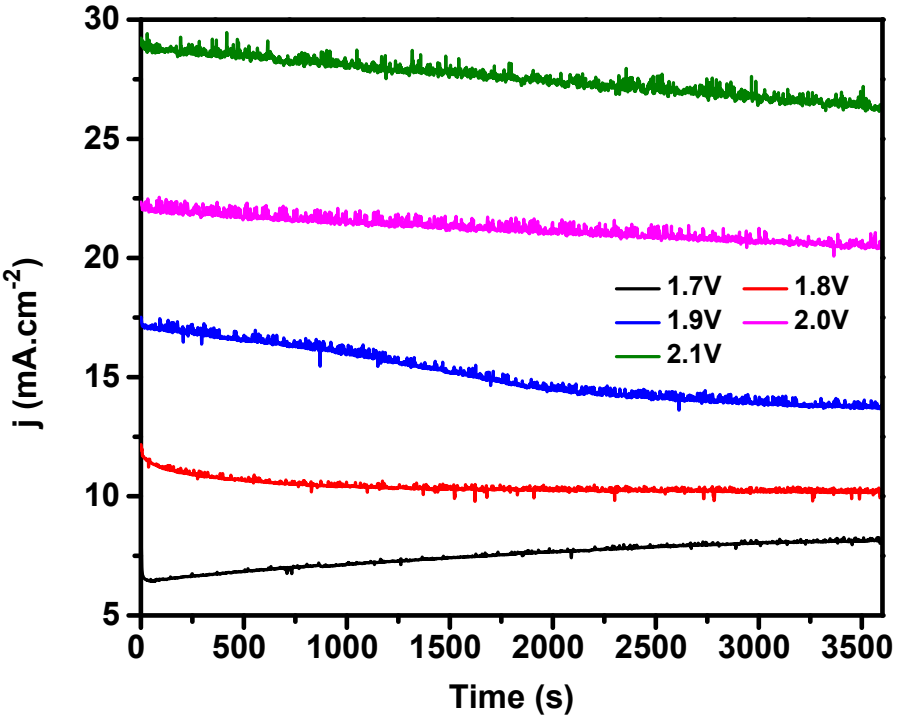

Figure S28. CPE analysis at various potentials in a 2-electrode system.

Table S1. Concentration of different elements in the electrolyte obtained from ICP-MS analysis during the long-term stability tests.

	Before electrolysis (mg/L)	**After electrolysis (mg/L)**
Bismuth (Bi)	0.16	0.96
Copper (Cu)	0.18	0.66
Cobalt (Co)	<0.005	<0.005